Trinity College Dublin
Coláiste na Tríonóide, Baile Átha Cliath
The University of Dublin

School of Engineering
Department of Mechanical & Manufacturing Engineering

Effect of the axial gap on the energy consumption of a single-blade wastewater pump

Federico Caruso and Craig Meskell

Published in Journal of Power and Energy (2020)

DOI: 10.1177/0957650920927366

Journal Title
XX(X):1–8
©The Author(s) 0000
Reprints and permission:
sagepub.co.uk/journalsPermissions.nav
DOI: 10.1177/ToBeAssigned
www.sagepub.com/
SAGE

Effect of the Axial Gap on the Energy Consumption of a Single-Blade Wastewater Pump

Federico Caruso[1] and Craig Meskell[1]

Abstract

The effect of the axial gap on the energy consumption of a single-blade wastewater pump (Sulzer XFP PE-2 150E CB1.1) is assessed using URANS simulations with ANSYS Fluent. The numerical model was compared to experimental data with a nominal design configuration (i.e. gap size) to provide confidence in the modeling approach. The global performance of the pump was evaluated in terms of pressure-discharge, torque and efficiency for a range of volumetric flow rates (110 $m^3 \cdot h^{-1}$ to 254 $m^3 \cdot h^{-1}$) and gap sizes (0.3 mm to 1.15 mm). While it is found that the power consumption at a given flow rate is reduced with increased gap, this is at the expense of a drop in outlet pressure, and hence the efficiency of the pump drops significantly. At the largest volumetric flow rate considered (254 $m^3 \cdot h^{-1}$), the sensitivity of the efficiency to the gap size is -13.5 $\% \cdot mm^{-1}$ and the sensitivity of the reduction in mechanical power consumption to gap size is 0.58 $kW \cdot mm^{-1}$. These results emphasize the importance of active maintenance during the lifetime of a wastewater pump to avoid a reduction in the energy performance caused by increased gap size.

Keywords

Efficiency, energy consumption, wasterwater pump

Introduction

Approximately 2 percent of the global world energy consumption is spent by electric motors to move, process and distribute industrial and municipal clean-water and wastewater[1]. Experience in the wastewater sector suggests that in some facilities between 25-50% of the energy input can be attributed to pumping[2], and around 20%-50% of the power consumed might be saved by varying the speed of the pumping systems[3]. Furthermore, the cost to operate a wastewater pump can be approximately half the total lifetime cost[4], reflecting the low capital cost relative to the energy cost. In this context, energy efficiency of the pump becomes important, not just to reduce the energy intensity of wastewater treatment, but also to reduce the cost. Degradation of the physical conditions of a pump during its lifetime may have a significant impact on the energy usage. Several authors assessed the actual operational global energy consumption in wastewater treatment plants and identified inefficiencies in pumps and aeration systems[5,6]. Recommendations to reduce the energy costs of such installations include load shifting to off-peak periods by using automated control systems and installation of variable frequency drives to manage pump cycle duties. In addition, the overall pump condition should be monitored indirectly by noting the average flow rate and energy consumption data over a period[5] and regular maintenance undertaken (typically once or twice per year) to reduce leakage in mechanical seals[7]. The emphasis on seals in maintenance protocols reflects the fact that the vibration induced by the impeller radial thrust can be severe due to the asymmetric nature of the impeller in waste water pumps. This radial loading can significantly shortening the life of bearings and seals thus affecting the device performance[18,19]. Proper maintenance, especially of the axial clearance between the impeller and the wear plate, which is shown in Fig. 1 as s_g, is not prioritized. It is commonly known that even small gaps between the rotating blades and the casing of turbomachinery in general can greatly influence performance[9–11]. For example, Liu et al.[14] investigated tip leakage in a multiblade pump as turbine (PAT) in pump mode, finding that the presence of the axial clearance causes unstable flow structure and complex vortex in the passage, decreasing head and efficiency. More in-depth studies focusing on the hydrodynamics of tip leakage vortex[15,16] found that the extent of flow instability is determined by the oscillation of tip leakage vortex and blade number. Hao et al.[17] found that tip leakage, especially for unsymmetrical clearances, affect pump cavitation performance, magnitude and direction of radial force. The principle design criterion for waste water pumps is resistance to blockage. As a result, the pumps are geometrically quite different to other radial and mixed flow pumps. They typically have a single-blade with very large chord and with a uniform height of volute. As a result, even a well maintained waste water pump operating optimally will have a significantly lower best efficiency than might be expected for other types of pump. While the importance of the tip clearance is well recognized for multi-blade pumps, there is less information available for single-blade wastewater pumps. In slurry pumps, which are similar

[1]Trinity College, Dublin, Ireland

Corresponding author:

Federico Caruso, Dept. of Mechanical and Manufacturing Engineering Trinity College, Dublin Ireland.

Email: carusof@tcd.ie

to wastewater pumps, Eugin et al.[12] found that increasing the blade clearance may drop the head and efficiency by up to 20%. De Souza et al.[13] carried out a limited assessment on the detrimental impact of the axial clearance for a single-blade pump, the authors state that it is impossible to eliminate due to manufacturing considerations. Based on the literature about multi-blade centrifugal pumps, it is to be expected that increased tip leakage will degrade the performance of wastewater pumps in terms of energy consumption. However, the purpose of this paper is to quantify the effect of the axial gap of a specific single-blade pump, which is typical of that found in industry.

Modelling

As the internal flow in waste water pumps is both strongly three-dimensional and unsteady it has been noted that CFD is a particularly beneficial research tool in investigating these devices[24]. Benra[20], compared the fluid-structure interactions using unsteady RANS based CFD with both k-ε and SST k-ω turbulence models. More recently, a series of papers by Pei et al.[21–23] documented an extensive study of a single-blade pump employing both experimental tests and numerical simulations with FEM and FVM computational methods. Again the focus of these papers was the vibrations induced by different flow regimes, especially for off-design conditions, where the radial loading has found to be more prevalent. These studies have not focused significantly on the effect of the hydrodynamics on the energy performance of wastewater pumps. Keays and Meskell[4], reported pump performance using commercial CFD solvers (FLUENT and CFX) and found good agreement with experimental data.

Geometry

The particular pump in this study is the XFP PE-2 150E CB1.1, designed and manufactured by Sulzer. This is typical of the sort of pump installed in municipal wastewater treatment plants and similar to pumps from other manufacturers (e.g. Xylem's Flygt, Grundfos). The hydrodynamic elements of the pump assembly consist of three main components: an adjustable wear plate, a single-blade impeller (with a base plate attached) and a double-curvature volute, shown in Fig. 1. The electric motor which would be installed below the volute casing (not shown in the figure) rotates the impeller about an axis aligned with the inflow direction. The impeller is a single-blade contra-block design with: a maximum diameter of 238 mm; a "ball passage" 100 mm wide; and a nominal design speed of 1450 rpm. The pump volute has a minimum and maximum radius of 166.91 mm and 223.46 mm respectively. The details of this part are shown in Fig. 2. The inflow and outflow inlets are 150 mm in diameter. The inflow entry has a rounded edge to allow the fluid to flow in smoothly as these pumps are often installed in a submerged tank without a draft pipe attached. The nominal distance between the impeller blade and the wear plate is set to 0.3 mm during ordinary operating conditions. However, this distance tends to increase during the machine life-cycle, potentially affecting the pump performance. The clearance can be adjusted using the mounting bolt system which secures the wear plate to the volute casing. However, this requires an active maintenance protocol.

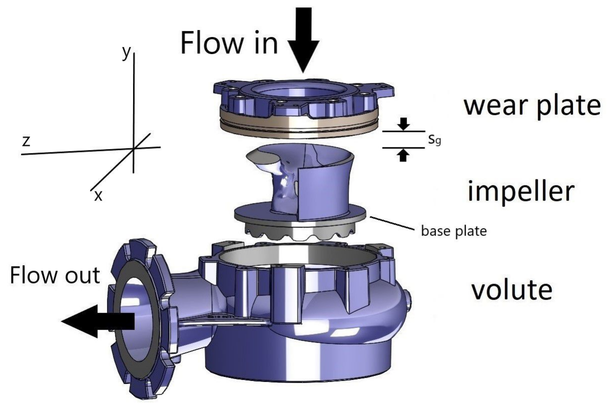

Figure 1. The axial gap, s_g, and the impeller base plate are indicated.

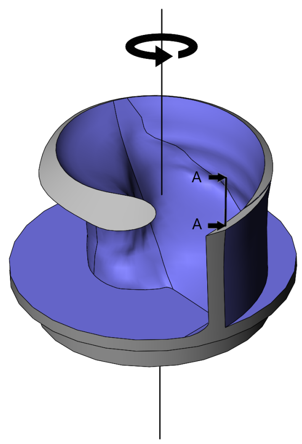

Figure 2. Detailed view of the impeller. Marked section A-A indicates location of data in Fig. 10.

For the following analysis, the 3D geometry that makes up the solid assembly has been simplified from the original design to facilitate meshing. In order to avoid compromising the simulated pump performance, only small modifications were made. This model attempts to balance performance accuracy with computational cost and was used to study the effect of the axial gap on the pump energy performance. The anti-clogging spiral groove on the wear plate has been suppressed and modelled as a flat surface. This feature has a depth 3 mm and may well influence the flow around the impeller as the gap is increased. The volute casing was left unchanged. The nominal design value for the gap between the wear plate and the impeller is 0.3 mm.

Mesh and numerical setup

An unstructured mesh, shown in Fig. 3 was applied to the fluid domain, shown in Fig. 4, resulting in tetrahedra to the main flow region, while a structured grid inflating in the pipe axis direction was used for the inlet and outlet

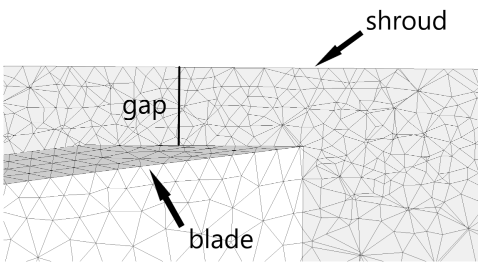

Figure 3. Computational mesh in the gap region.

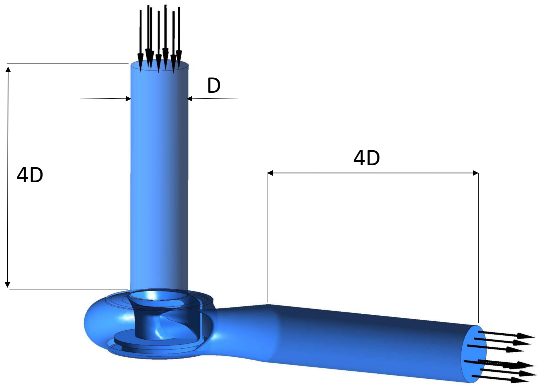

Figure 4. Computational domain.

pipes to reduce the cell count. Refinements near the rotating surfaces were required to capture the flow around the rotating walls. The different geometry configuration associated with the range of axial gap clearances resulted in a mesh count between 2.6 and 4.6 million cells. A grid independence study considering three different refinements showed no significant variation ($<2\%$) in the bulk output quantities (e.g. pressure head, torque, efficiency) with increased mesh density. The following results are presented with the finest grid to ensure more reliable numerical accuracy. The y^+ values range from 30 to 300 on the static walls, with an average of 200 on the rotating region. Therefore, the near-wall region can be considered to be resolved for the purpose of URANS equations. A temporal discretization conducted for an impeller rotation angle of 1°, 3° and 6° showed that 3° is sufficiently fine to ensure that head and power deviations are lower than 2%. A convergence criterion consisting of three sub-criteria is applied to address the validity of the numerical solutions, showing that residuals for continuity and momentum drop at least five orders of magnitude, while global mass flow imbalance and averaged bulk output quantities between successive revolutions are below 1%. A similar approach was adopted by Melzer et al.[26], concluding that it is sufficient for the validation of the numerical solution. The CFD software used for the numerical simulations was ANSYS FLUENT 19.2. Three-dimensional URANS equations are solved in a pressure-based first order implicit transient formulation. Turbulence closure was achieved using a realizable k-ε model, with non-equilibrium wall functions. Time stepping was achieved using the segregated PISO algorithm without skewness-neighbour coupling. Pressure, momentum and turbulent quantities were based on a second order upwind spatial resolution. The working fluid is incompressible water at ambient conditions. Residual convergence criteria were set to 10^{-3} for continuity and momentum and 10^{-5} for turbulent kinetic energy and turbulent dissipation ratio. The torque was calculated with respect to the impeller rotation axis. The pressure head developed was obtained by monitoring the area-weighted average values of the static pressure on the inlet surface, setting zero gauge pressure on the outlet pipe extremity as a boundary condition. The impeller and the inlet pipe fluid rotated at 1475 rpm relatively to the stationary volute and outlet pipe.

The axial flow velocity was specified on the inlet boundary, and so the mass flow rate is controlled directly. Fifteen rotations were needed to achieve periodic behaviour in the head. The position increment was set to an angular displacement of 3° by using a time step size of 3.39×10^{-5}s.

Results

Effect of the gap on pump performance

In order to assess the behaviour of the wastewater pump due to impeller-wear plate gap variation, the numerical model was run for six prescribed mass flow rates. The rotational speed was set at the nominal design speed of 1475 rpm. The axial gap s_g was varied from the design value of 0.3 mm to 0.6 mm in increments of 0.1 mm. in order to assess if the trend in the performance curves will extend to larger gaps, a value of 1.15 (nearly 4 times the design values) is also simulated. Fig. 5a shows the simulated head-discharge curve compared with the experimental data. The head-discharge, torque and efficiency curves have been provided from the manufacturer following in-house test on the hydraulic machine, according to the ISO9906:2012. The numerical values, are averaged over the final revolution. The head-discharge curve at 0.3 mm obtained from simulations approaches the experimental data with an under prediction of approximately 1.7 m at low flow rates and 3 m at high flow rates and at 198 $m^3 \cdot h^{-1}$ (which corresponds to the Best Efficiency Point). As would be expected, as the gap is increased, the developed head decreases at each flow rate. This is manifested as a drop of the back pressure at the inlet interface, which is caused by leakage around the tip of the impeller. Another interpretation of the performance reduction may be that the numerical model does not capture adequately how kinetic energy is converted to pressure and transferred to the fluid. This is indicated by the higher discrepancy at higher flow rates, where the model is not able to represent the flow unsteadiness adequately. The same phenomenon has already been observed in literature[13], although the fluid dynamics was not addressed by a thorough narrative. The hydraulic efficiency, shown in Fig. 5c, is specified as the ratio of difference of hydraulic power between inlet and outlet (i.e. effectively the stagnation pressure increase) to the shaft power applied to the impeller. It should be noted that the experimental value is based on the electricity consumption of the motor, and so embeds a simple estimate of electrical and mechanical losses. On the other hand, the efficiency obtained in the simulations calculates the hydraulic power input directly for the torque acting on the impeller. The effect of the gap observed in the numerical data is to move the maximum efficiency seen in Fig. 5c from 198 $m^3 \cdot h^{-1}$ at 0.3 mm to 170 $m^3 \cdot h^{-1}$ at 1.15 mm. For the gaps in between, the maximum is at 230 $m^3 \cdot h^{-1}$.

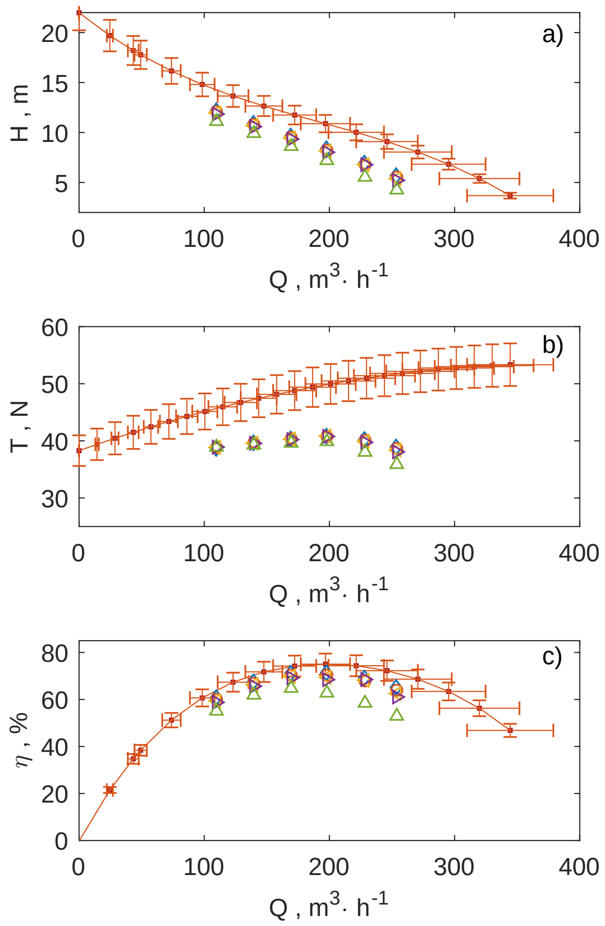

Figure 5. Variation of pump performance metrics with volumetric flow rate for different gaps: a) Pressure Head-Flow rate, b) Average torque about impeller rotation axis, c) Hydraulic efficiency (□ Experimental data; ◇ 0.3 mm; ○ 0.4 mm; ◁ 0.5 mm; ▷ 0.6 mm; △ 1.15 mm).

Fig. 5b reports the average torque for different gaps compared with experimental data. Interestingly, the largest changes in the momentum occur for flow rates higher than the best efficiency point. Conversely, the maximum torque at 110 $m^3 \cdot h^{-1}$ is shown for 1.15 mm gap. This is in contrast to what is observed for the pressure head, where the developed head constantly decreases as the gap is increased. It should be remembered that the torque is calculated as the area-weighted average of the pressure and viscous forces acting on the faces of the rotating body. Therefore, it represents the energy exchange between the rotating walls and the fluid. Nevertheless, the momentum drop observed at high flow rates is perhaps due to the over-prediction of the viscous forces.

Fig. 6a shows the variation of the pump efficiency at the same flow rate with the gap. The efficiency is higher when the pump operates at flow rates around the best efficiency point, and is lower at higher and lower pressure head, as would be expected. However, for gaps greater than 0.5 mm the estimated flow rate for best efficiency point is 170 $m^3 \cdot h^{-1}$, rather than 198 $m^3 \cdot h^{-1}$ as found for the nominal design gap of 0.3 mm.

As can be seen in Fig. 5c, the efficiency drops significantly with increased gap. At a flow rate of $Q = 230$ $m^3 \cdot h^{-1}$ the efficiency is reduced by 13.5 percentage points for a gap size $s_g = 1.15mm$ compared with the nominal design configuration. Generally, the efficiency data for all flow rates exhibit a downward trend with increased gap size. However, at a flow rate of 230 $m^3 \cdot h^{-1}$ the data exhibits an increase in efficiency around a gap size of 0.5 mm and 0.6 mm. It is tempting to simply claim this as a numerical artifact. However, the deviation from the trend occurs in two independent simulations ($s_g = 0.5$mm and $s_g = 0.6$mm) each with an independently generated mesh and furthermore, at the largest gap size ($s_g = 1.15$mm) , the behaviour at this flow rate returns to the expected trend. While this behaviour may well be due to a numerical interaction, it could also be due to a physical phenomenon. As the gap is increased at a specific flow rate, the local flow around the gap will be prone to shear layer instability, analogous to vortex shedding. In other turbomachinery, this can give rise to so-called non-synchronous vibration[27]. While the time and spatial scale of this phenomenon would be too high to be fully captured with the current model resolution, such behaviour would act as a blockage, reducing leakage flow and increasing apparent efficiency. Clearly, further work is needed to investigate this anomaly, but the overall trend in Fig. 6a is clear.

Sensitivity of performance to gap size

While the efficiency is already a non-dimensional quantity, to facilitate comparison with the nominal design configuration, the efficiency can be normalised relative to a reference configuration. Fig. 6b shows the normalised efficiency expressed as the ratio of the efficiency η presented in Fig. 6a to a reference efficiency η_{ref} chosen as $s_g = 0.3$ mm. Similarly, the gap s_g is normalised with respect to a reference gap length s_{ref}. It is seen that as the flow rate and the gap size increase, the efficiency ratio drops to 0.91 at 140 $m^3 \cdot h^{-1}$ and to 0.82 at 254 $m^3 \cdot h^{-1}$ when the gap is 1.15 mm. The efficiency ratio drop follows a linear downward trend for each flow rate. The sensitivity of the efficiency ratio to increase in gap size can be captured as a sensitivity factor K, defined as:

$$K(Q) = \overline{\left(\frac{\partial \frac{\eta}{\eta_{ref}}}{\partial \frac{s_g}{s_{ref}}} \right)} \tag{1}$$

The non-dimensional parameter K defined in Eqn. 1 is obtained by linear regression of a straight line to the normalised quantities shown in Fig. 6b for constant Q. As a result, they are a functions of the flow rate. The coefficient of determination, r^2, is greater than 99% for all flow rates except 230 $m^3 \cdot h^{-1}$, where it drops to 90% due

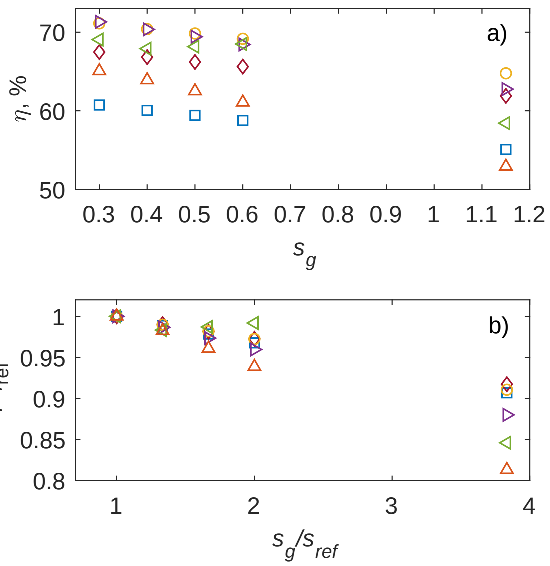

Figure 6. Variation of efficiency with gap size for a range of flow rates: a) Variation of efficiency, η, with gap size, b) Normalised efficiency with normalised gap (□ 110 $m^3 \cdot h^{-1}$; ◇ 140 $m^3 \cdot h^{-1}$; ○ 170 $m^3 \cdot h^{-1}$; ▷ 198 $m^3 \cdot h^{-1}$; ◁ 230 $m^3 \cdot h^{-1}$; △ 254 $m^3 \cdot h^{-1}$).

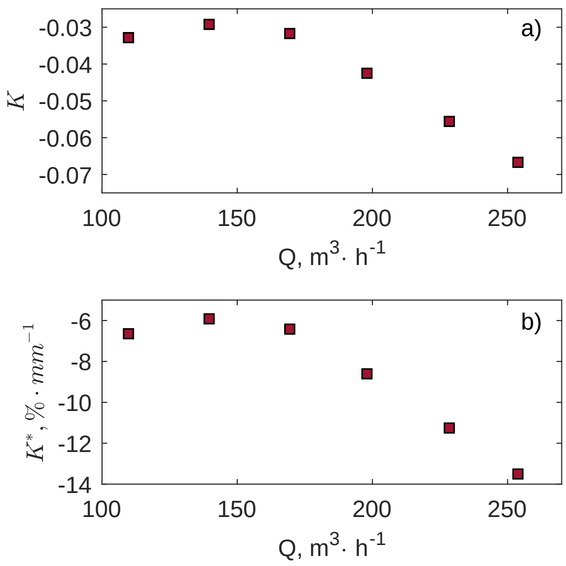

Figure 7. Sensitivity of efficiency to gap size: a) Variation of non-dimensional sensitivity K with flow rate, b) Variation of efficiency sensitivity factor K^* with flow rate.

to the behaviour previously noted around $s_g/s_{ref} = 2$. The trend for K is plotted in Fig. 7a, signifying that the efficiency becomes more sensitive. It is seen that K increases up to Q =140 $m^3 \cdot h^{-1}$ and decreases at higher rates.

It is also possible to define a dimensioned sensitivity factor K^* as:

$$K^*(Q) = K(Q) \cdot \frac{\eta_{ref}}{s_{ref}} = \overline{\left(\frac{\partial \eta}{\partial s_g}\right)} \qquad (2)$$

The parameter K^*, defined in Eqn. 2 and shown in Fig. 7b, has units $\% \cdot mm^{-1}$ and quantifies the sensitivity of efficiency to increased gap length in millimetres for each flow rate. The sensitivity is always negative, indicating that increasing gap size will always cause a degradation in pump performance.

The variation of power consumed with increased gap size is more complicated. Fig. 8a shows the mechanical power consumed at each flow rate and gap size. In order to compare flow rates, the power can be normalized by the power consumed at the nominal design gap ($s_g = 0.3$ mm) for each flow rate. This is plotted against the normalized gap size in Fig. 8b. As before, the data follows a linear trend for each flow rate. A sensitivity factor $\tilde{K}$ and $\tilde{K}^*$ can be defined:

$$\tilde{K}(Q) = \overline{\left(\frac{\partial \frac{P_m}{P_{ref}}}{\partial \frac{s_g}{s_{ref}}}\right)} \qquad (3)$$

$$\tilde{K}^*(Q) = \tilde{K}(Q) \cdot \frac{P_{ref}}{s_{ref}} = \overline{\left(\frac{\partial P_m}{\partial s_g}\right)} \qquad (4)$$

The parameter $\tilde{K}$ is non-dimensional while $\tilde{K}^*$ has units kW$\cdot$ mm^{-1} indicating the change in power requirement due to increased gap at each flow rate. The variation of $\tilde{K}$ and $\tilde{K}^*$ are shown in Fig 9.

Except for the lowest flow rate, both $\tilde{K}$ and $\tilde{K}^*$ are negative,

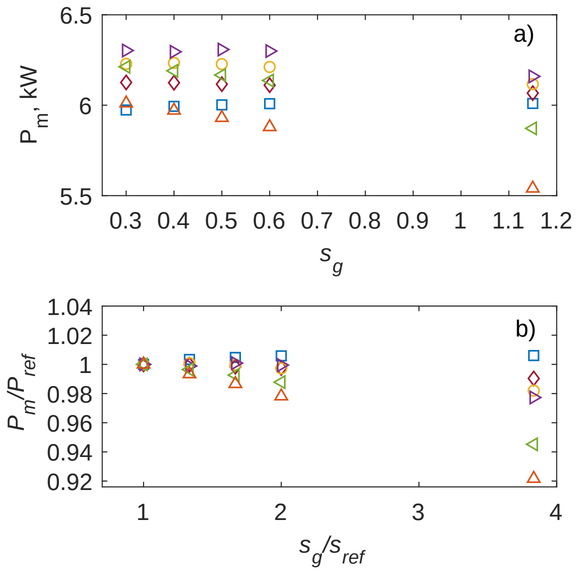

Figure 8. Variation of mechanical power consumption with gap size for various flow rates: a) Mechanical power consumption, b) Mechanical power normalized by a reference power (□ 110 $m^3 \cdot h^{-1}$ ◇ 140 $m^3 \cdot h^{-1}$ ○ 170 $m^3 \cdot h^{-1}$ ▷ 198 $m^3 \cdot h^{-1}$ ◁ 230 $m^3 \cdot h^{-1}$ △ 254 $m^3 \cdot h^{-1}$).

indicating a drop in power required to sustain the flow rate as gap size increases. This is due to a drop in viscous loss between the blade and the wear plate. At a flow rate of 254 $m^3 \cdot h^{-1}$, the power consumption at $s_g = 1.15$ mm drops by 0.58 kW. However, it is worth noting that this reduction in power, which at first may seem advantageous, is achieved with a drop in output pressure head due to leakage, and so there is a drop in efficiency. In practice, this will mean that the flow-rate will be reduced to meet the head requirement,

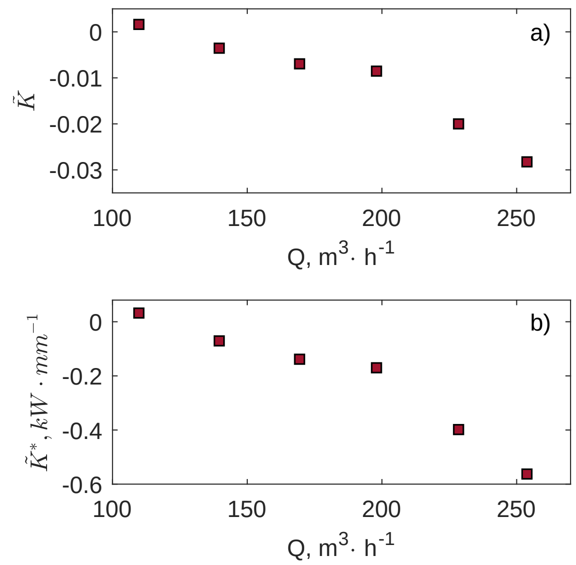

Figure 9. Sensitivity of mechanical power consumed P_m to change in the gap size s_g: a) Variation of non-dimensional sensitivity factor $\tilde{K}$ with flow rate, b) Variation of sensitivity factor $\tilde{K}^*$ with flow rate.

necessitating the pump to run for longer and hence draw more energy.

In an attempt to understand better the impact of the gap on the pump performance, the cylindrical velocity components, time averaged over a single revolution, are reported in Fig. 10 for a range of gaps and two flow rates. The data is taken on section A-A in Fig. 2 which is normal to the wear plate at the midpoint between the pressure and suction side of the impeller. The section location is fixed relative to the impeller. The velocities are normalised with respect to the inlet velocity u_i and the location, s, in the gap, is normalized by the gap size, s_g.

The average mass flow in the axial direction must be zero because of the solid boundaries. The non-zero axial velocities shown in Fig.10a are due to the particular location of section A-A and the fact that it is body fixed to the impeller. A Lagrangian assessment of the fluid flow would show a particle of fluid being swept upwards as the impeller blade advances, through the gap and then downwards as the impeller passes. The radial velocity (Fig. 10b) is dominated by the flow rate. Note that although the normalised radial velocity is comparable for all gap sizes, the radial volumetric flow rate (i.e. the leakage) will be larger for bigger gaps and will vary linearly with gap size. This explains the linear reduction in efficiency with gap size. Curiously, at this location, the radial velocity which is more negative for higher flow rates indicates higher leakage. This is counter-intuitive as high flow rates are associated with low pressure difference across the impeller, and hence one might expect lower leakage. On average this will be the case over the entire length of the impeller, but close to the trailing edge, the flow will experience large vortex structures, which will be dominated by inertial effects. The tangential velocity component (Fig. 10c) is insensitive to either gap size or flow rate. It is proposed that the tangential component is determined by the rotational speed, but as only one speed has been simulated here, further work is needed to verify this. The trend in Fig. 10b shows three linear sections. One might be concerned that the central region with almost constant velocity is a consequence of mesh design. However, this has been investigated and there is no evidence that this is the case. Moreover, each gap size represents a completely different mesh, both in terms of cell count and distribution. The torque associated with shear stress at the impeller depends on the spatial gradient of the tangential velocity at $s = 0$. The fact that the normalised tangential velocity collapses well in Fig. 10c implies that the shear stress will scale linearly with both gap size (s_g) and flow rate (u_i), which is consistent with the linear trend of the power consumption with gap size and the linear trend of the power sensitivity factor $\tilde{K}$.

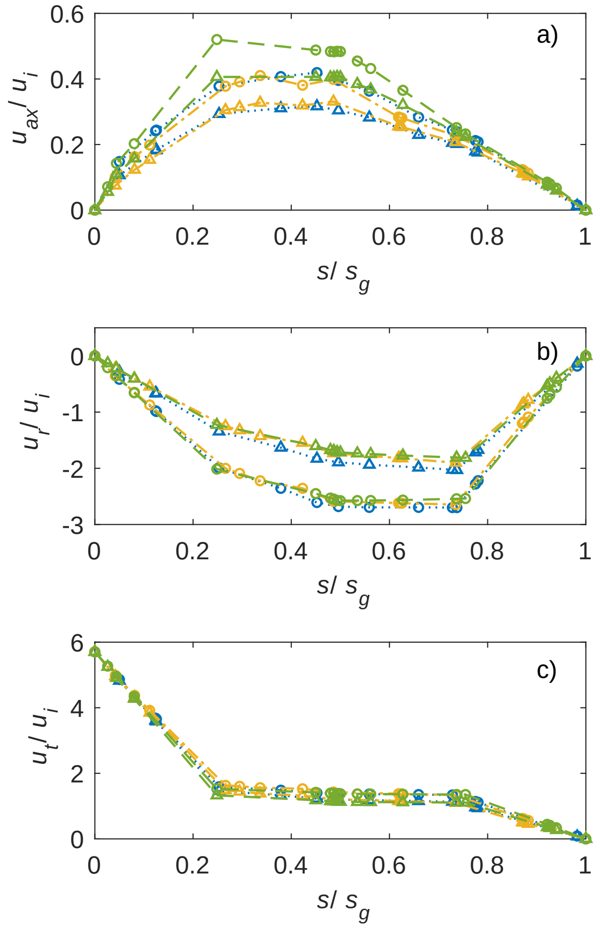

Figure 10. Variation of velocity components in the gap region for different gaps and flow rates: a) Axial velocity, b) Radial velocity, c) Tangential velocity (· · · △ · · · 0.3 mm, 110 m^3·h^{-1}); · · · ○ · · · 0.3 mm, 254 m^3·h^{-1}; – · △ · – 0.5 mm, 110 m^3·h^{-1}; – · ○ · – 0.5 mm, 254 m^3·h^{-1}; – △ – 1.15 mm, 110 m^3·h^{-1}; – ○ – 1.15 mm, 254 m^3·h^{-1}).

Conclusions

An assessment of the axial gap on the energy consumption of a single-blade wastewater pump has been accomplished through three-dimensional unsteady numerical simulations. The pump performance is found to be degraded by increases in the gap size, with the largest drop in efficiency reported as 13.5%. While it is true that for a given flow rate the power consumption is reduced, this is associated with a decrease in the pressure head. The sensitivity of both the efficiency and the power consumption to gap size is found to be linear, allowing sensitivity factors to be quantified. This is consistent with the local flow field in the gap region. Non-dimensional sensitivity factors have also been produced, as this will allow the results to be applied to similar pumps or different sizes. Although the effect of gap size on energy performance of a wastewater pump is smaller than the reported benefit of variable speed drives, it is potentially significant. Therefore, it is concluded that as well as the capital intensive strategies to improve total pump efficiency, such as variable speed drives, it is important to implement a proactive maintenance protocol throughout the lifetime of the installation.

Acknowledgements

This work has been carried out with the aid of ESIPP which is financially supported by Science Foundation Ireland under the SFI Strategic Partnership Programme (Grant Number SFI/15/SPP/E3125), five industry members of UCD Energy institute and a philanthropic donation by the chair of UCD Energy Institute, Mr. David O'Reilly. The authors wish to acknowledge the DJEI/DES/SFI/HEA Irish Centre for High-End Computing (ICHEC) for the provision of computational facilities and support. The authors also would like to thank Mr. Ben Breen and his staff at Sulzer Ltd.

References

1. Lawrence National Laboratory. "Improving Pumping System Performance A Sourcebook for Industry. Technical report, U.S. Department of Energy and Resource Dynamics Corporation, 2006.
2. EUROPUMP. Variable speed pumping: A guide to successful applications. *Elsevier Science*, 2004.
3. V. K Gaudani. *Energy Efficiency in Electrical Systems (1st Ed.)*. IECC Press, 2009.
4. J. Keays and C. Meskell. A study of the behaviour of a single-bladed waste-water pump. *IMechE Journal of Process Mechanical Engineering*, 220(2):79–87, 2006.
5. D. Torregrossa, G. Schutz, A. Cornelissen, F. Hernández-Sancho, J. Hansen . Energy saving in WWTP: daily bench-marking under uncertainty and data availability limitations *Applied Energy*, 208:1430–1440, 2016.
6. J. Krampe. Energy benchmarking of South Australian WWTPs. *Water Sci Technol*, 67 (9): 2059—2066, 2013.
7. NYSERDA. Water & wastewater energy management. *New York State Energy Research and Development*, 2010.
8. Hydraulic Institute and Department of Energy (US). Improving pumping system performance: a sourcebook for industry. *Technical Report*, 2006.
9. G. M. Wood, H. Welna, and R. P. Lamers. Tip clearance effects in centrifugal pumps. *ASME Journal of Fluids Engineering*, 87:932–940, 1965.
10. W. Zhou, Z. Zhao, T. S. Lee, and S. H. Winoto. Investigation of flow through centrifugal pump impellers using computational fluid dynamics. *International Journal of Rotating Machinery*, 9(1):49–61, 2003.
11. C. Lei, Z. Yiyang, W. Zhengwei, X. Yexiang, and L. Ruixiang. Effect of the axial clearance on the efficiency of a shrouded centrifugal pump. *ASME Journal of Fluid Engineering*, 137(071101):1–10, 2015.
12. T. Engin and M. Gur. Performance characteristics of a centrifugal pump impeller with running tip clearance pumping solid-liquid mixtures. *ASME Journal of Fluids Engineering*, 123(3):532–538, 2001.
13. B. De Souza, J. Daly, A. Nive, and P. Frawley. Numerical simulation of transient flow through single blade centrifugal pump impellers with tipgap leakage. *Proceedings of the 4th WSEAS International Conference on Fluid Mechanics and Aerodynamics, Elounda, Greece*, pages 349–354, 2006.
14. Y. Liu and L. Tan. Tip clearance on pressure fluctuation intensity and vortex characteristic of a mixed flow pump as turbine at pump mode. *Renewable Energy*, 129:606-615, 2018.
15. Y. Liu and L. Tan. Spatial-temporal evolution of tip leakage vortex in a mixed-flow pump with tip clearance. *Journal of Fluids Engineering, Transactions of the ASME*, 141(8):1–11, 2019.
16. Y. Liu and L. Tan. Theoretical Prediction Model of Tip Leakage Vortex in a Mixed Flow Pump with Tip Clearance. *Journal of Fluids Engineering, Transactions of the ASME*, 142:1–11, 2019.
17. Y. Hao and L. Tan. Symmetrical and unsymmetrical tip clearances on cavitation performance and radial force of a mixed flow pump as turbine at pump mode. *Renewable Energy*, 127:368–376, 2018.
18. T. Okamura. Radial thrust in centrifugal pumps with a single-vane impeller. *Bulletin of the JSME*, 23(180):369–375, 1980.
19. M. Aoki. Instantanous interblade pressure distributions and fluctuating radial thrust in a single- blade centrifugal pump. *Bulletin of the JSME*, 27(223):369–375, 1984.
20. F. K. Benra. Numerical and experimental investigation on the flow induced oscillations of a single-blade pump impeller. *ASME Journal of Fluids Engineering*, 128(4):783–793, 2006.
21. J. Pei, F. K. Benra, and H. J. Dohmen. Investigation of unsteady flow-induced impeller oscillations of a single-blade pump under off-design conditions. *Journal of Fluids and Structures*, 35:89–104, 2012.
22. J. Pei, S. Yuan, F. K. Benra, and H. J. Dohmen. Numerical prediction of unsteady pressure field within the whole flow passage of a radial single-blade pump. *Journal of Fluids Engineering*, 134(10):101103 1–11, 2012.
23. J. Pei, S. Yuan, X.-J. Li, and W. Wang. Numerical prediction of 3-d periodic flow unsteadiness in a centrifugal pump. *Journal of Hydrodynamics*, 26(2):257–263, 2014.
24. A. M. Hamiche, A. B. Stambouli, and S. Flazi. A review of the water-energy nexus. *Renewable and Sustainable Energy Reviews*, 65:319–331, 2016.
25. J. F. Gulich. *Centrifugal Pumps*. Springer, 2nd ed., 2008.
26. S. Melzer, T. Muller, S. Stephan, K. Tobias, S. Romuald. Experimental and numerical investigation of the transient characteristics and volute casing wall pressure fluctuations

of a single-blade pump. *Proceedings of the Institution of Mechanical Engineers, Part E: Journal of Process Mechanical Engineering*.

27. S T. Clark, R E. Kielb, and K C. Hall. A Van Der Pol based reduced-order model for non-synchronous vibration (NSV) in turbomachinery. *Proceedings of ASME Turbo Expo 2013: Turbine Technical Conference Exposition, San Antonio, Texas, USA*, June 3–7, 2013.